Sustainable Energy & Fuels

ROYAL SOCIETY OF CHEMISTRY

PAPER

View Article Online
View Journal | View Issue

Cite this: *Sustainable Energy Fuels*, 2024, **8**, 1549

Long-term performance of hydrogen-bromine flow batteries using single-layered and multi-layered wire-electrospun SPEEK/PFSA/PVDF membranes

Sanaz Abbasi,[ab] Yohanes Antonius Hugo,[b] Zandrie Borneman,[ac] Wiebrand Kout[b] and Kitty Nijmeijer*[ac]

Sulfonated poly (ether ketone) (SPEEK), perfluorosulfonic acid (PFSA), and polyvinylidene fluoride (PVDF) were wire-electrospun. Subsequently, multiple electrospun layers in different arrangements were hot-pressed into sustainable membranes for use in hydrogen-bromine flow batteries (HBFBs). The relationship between the electrospun layer composition and arrangement, membrane properties, and battery performance was explored. Wire-electrospinning and hot-pressing improved SPEEK and PFSA/PVDF compatibility, yielding dense membranes. Higher SPEEK contents lead to rougher morphologies, while the insulating nature of PVDF decreases the ion exchange capacity (IEC) and HBr uptake compared to commercial PFSA. The multi-layer assembly negatively impacted the membrane transport properties compared to the single-layer arrangement. Although wire-electrospinning improves the polymer dispersion and fixed charge density, SPEEK-rich regions of the blend membranes lack the high selectivity of PFSA, thus reducing the ionic conductivity. This is especially clear in the multi-layer membranes with accumulated SPEEK in the intermediate layer in the through-plane direction. Following initial property comparisons, thinner wire-electrospun SPEEK membranes were prepared with area resistance in the PFSA-comparable range. Among the wire-electrospun SPEEK/PFSA/PVDF membranes, the single-layered membrane with 8 wt% SPEEK (SPF1-8; 62 μm) displayed stable HBFB performance at 200 mA cm^{-2} over 100 cycles (64 cm^2 active area). Based on the ex-situ measurements and cell performance results, a total of ~10.5 wt% SPEEK is suggested as the limit for both single and multi-layered wire-electrospun membranes, combined with a maximum membrane thickness of ~50 μm. This ensures robust HBFB performance, positioning wire-electrospun SPEEK/PFSA/PVDF membranes as a PFSA alternative in energy storage.

Received 20th December 2023
Accepted 26th February 2024

DOI: 10.1039/d3se01670f

rsc.li/sustainable-energy

Introduction

By 2050, electricity demand is set to triple due to the electrification of society and the use of hydrogen-based fuels to reduce carbon emissions. Renewable energy, led by substantial solar and wind power growth, is expected to make up 80–90% of the global energy mix. Furthermore, there could be a fivefold increase in the demand for hydrogen by 2050, along with a rise in the use of sustainable fuels.[1] However, the inherent intermittency of renewable energy sources, such as solar and wind power, accentuates an imperative need for dependable, efficient, and economically viable energy storage technologies.[2]

In the domain of electrochemical systems, redox flow batteries (RFBs) stand out as an environmentally friendly resource, seamlessly integrating swift reaction time coupled with remarkable efficiency.[3,4] Promisingly addressing the flexibility of RFBs, hydrogen-bromine flow batteries (HBFBs) offer the potential for high power output alongside cost-effectiveness. The robust power performance of HBFBs is attributed to the swift kinetics of the bromine redox couple that contribute to outstanding energy efficiency and prolonged operational duration.[3,5]

HBFB systems consist of two distinct dual tanks: one housing an aqueous HBr/Br_2 solution, while the other accommodates H_2 storage. The overall electrochemical reaction that takes place within the cell involves the oxidation of hydrogen gas at the anode and the reduction of bromine species at the cathode:[6]

$$H_2 + Br_{2(aq.)} \underset{\text{Charge}}{\overset{\text{Discharge}}{\rightleftharpoons}} 2HBr_{(aq.)} \quad E_{0,\,cell} = 1.098\ V \qquad (1)$$

[a]*Membrane Materials and Processes, Department of Chemical Engineering and Chemistry, Eindhoven University of Technology, P.O. Box 513, 5600 MB Eindhoven, The Netherlands. E-mail: D.C.Nijmeijer@tue.nl*

[b]*Elestor B.V., P.O. Box 882, 6800 AW Arnhem, The Netherlands*

[c]*Dutch Institute for Fundamental Energy Research (DIFFER), P.O. Box 6336, 5600 HH Eindhoven, The Netherlands*

This results in the generation of electricity when needed and the subsequent recharging of the battery during surplus energy availability.

Wang *et al.*[7] showed that Br_2 rapidly dissolves in the HBr solution through the formation of tribromide (Br_3^-):

$$Br_2 + Br^- \overset{K}{\rightleftharpoons} Br_3^- \quad (2)$$

where $K = 16$ is the equilibrium constant at 25 °C.

This dynamic interplay of chemical reactions enables HBFBs to effectively store and release energy as required, making them attractive for various energy storage applications.[3,8]

Contrary to the rapid bromine species reactions, the rate of hydrogen oxidation and evolution reactions (HOR/HER) heavily depends upon the presence of the catalyst at the gas diffusion electrode (GDE) surface to enhance the performance and control the costs.[9]

In order to accelerate the hydrogen oxidation and evolution reactions (HOR/HER) while concurrently preventing the migration of bromine species (predominantly Br_2 and Br_3^-) to the hydrogen electrode, a combination of a catalyst-coated GDE and an ion-exchange membrane, collectively known as the membrane-electrode assembly (MEA) is essential.[10] The ion-exchange membrane facilitates the movement of protons, thereby promoting the desired reactions, while simultaneously impeding the unwanted passage of Br_2 and Br_3^- to the GDE. Thus, an optimal proton-conductive membrane contributes to fine-tuning the electrochemical reactions and enhances the battery efficiency.[6]

In HBFB technology, three pivotal attributes-high peak power density, prolonged operational lifespan and economical cost per kW h of supplied electricity-emerge as the most critical factors.[11] Achieving the right equilibrium among these vital characteristics is essential for membrane optimization, ensuring a superior HBFB performance and durability while maintaining competitive costs.[6,10,12] Efforts to enhance the ion selectivity and minimize the ohmic resistance of the membrane in the hydrogen-bromine systems have initiated numerous investigations. Existing research predominantly focuses on the utilization of perfluorosulfonic acid (PFSA) polymer, notably Nafion®, as a dense proton-conductive membrane.[6,8,10,13–16] However, PFSA membranes, despite their commendable proton conductivity and resistance against bromine species, display an elevated water uptake. This phenomenon enhances the diffusion rate of bromine and the consequent poisoning of the hydrogen catalyst, while simultaneously causing a decrease in the electrolyte concentration during charging.[10,17] Moreover, the significant cost contribution of PFSA membranes to the overall materials expense (reported at 38%),[8,18] coupled with environmental concerns, underlines the need to develop a high-performing and environmentally conscious membrane at a low cost.

Hugo *et al.*[6] extensively investigated diverse membrane chemistries, both as alternatives to commercial PFSA and as PFSA-blended compositions in order to reduce the overall membrane costs, specifically for HBFB applications. The study involved a range of commercial membranes, including sulfonated polyvinylidene fluoride (SPVDF). However, none demonstrated a superior combination of durability and performance when compared with PFSA. In a separate study,[5] Hugo *et al.* explored wire-electrospun PFSA/PVDF blends, a concept previously introduced by Park *et al.*[19] Their findings identified a 50/50 PFSA/PVDF composition, with a wet thickness of approximately 100 μm, as most optimal in agreement with the benchmark PFSA performance over 200 cycles at a current density of 150 mA cm^{-2}. Despite this encouraging result, the 50 wt% PFSA contribution in conjunction with the relatively high membrane thickness still presented an elevated PFSA contribution. This issue underscores the dual necessity to reduce PFSA usage to mitigate the environmental impacts and optimize the membrane cost.

Concurrently with the research done by Hugo *et al.*,[5] our previous work[20] delved into the development of a novel, comparably eco-friendly proton-exchange membrane through the same wire-electrospinning technique followed by a final hot-pressing step. In that study, we used sulfonated poly (ether ketone) (SPEEK), an accessible hydrocarbon-based proton-conductive polymer, renowned for its low cost compared to Nafion®. The use of SPEEK translated into a 27% reduction in the total materials expense. Building on the foundation laid by earlier studies[21–24] involving SPEEK/PVDF and SPEEK/PFSA blends, as well as Park *et al.*'s contribution,[12] we then integrated PVDF as a perfluorinated, mechanically and economically robust polymer. This integration successfully controlled the bromine species crossover and cut down costs with PVDF being over 200 times cheaper than Nafion®.[25] Notably, the HBFB single cell exhibited optimal polarization behavior and ohmic resistance upon deploying the wire-electrospun membrane comprising an 80/20 (wt%/wt%) SPEEK/PVDF ratio. However, the marginal thickness (~50 μm) coupled with the limited chemical/mechanical stability of the substantial SPEEK portion prompted a swift decline in the HBFB cycling performance.

The first results of electrospun SPEEK/PVDF and SPEEK/PFSA membranes thus show promise for this concept, but the build-up of the different layers in the membrane was rather straightforward. Furthermore, the vulnerability of SPEEK, whether used alone or in combination with PVDF, to bromine species motivates us to investigate the role of PFSA in protecting SPEEK against bromine-induced degradation. In this work, we now build on this concept and carefully combine and integrate SPEEK, PFSA, and PVDF electrospun polymer layers and transform these into composite membranes using hot-pressing (Fig. 1). To strategically manage membrane costs and limit the use of PFSA, the total PVDF content was precisely calibrated at 50 wt% with a membrane thickness of only 30 μm to 60 μm, whereas the amount of SPEEK instead of PFSA as proton conductive material was varied. The feasibility of intertwining SPEEK, PFSA and PVDF as a tool to balance membrane swelling, ionic conductivity and stability with the ultimate aim of maximizing battery performance was evaluated (Fig. 1a and b). Parallel to the variation in SPEEK/PFSA/PVDF composition, we investigated the effect of the sequence of electrospun layer arrangement (Fig. 1c) on the membrane properties, HBFB

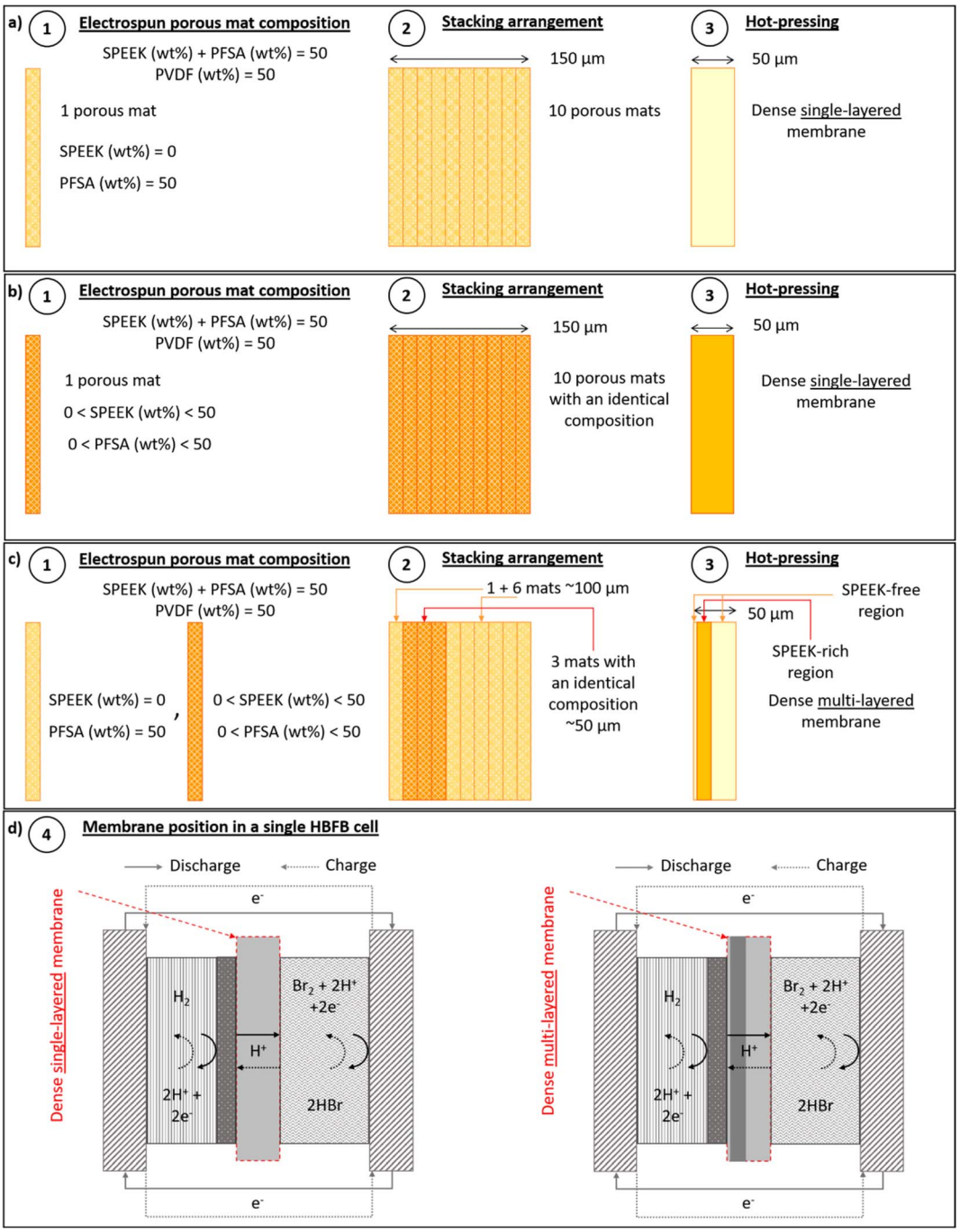

Fig. 1 Illustration of the SPEEK/PFSA/PVDF wire-electrospun mats composition and arrangement before and after hot-pressing: (a) and (b) single-layered membranes; (c) multi-layered membranes with (d) the visual position of the final membrane in a single HBFB cell.

single-cell (Fig. 1d) performance and especially membrane lifetime.

Experimental

Electrospinning

SPEEK/PFSA/PVDF blend fiber mats were fabricated *via* the electrospinning of blend solutions incorporating varying ratios of SPEEK, PFSA and PVDF in *N*,*N*-dimethylformamide (DMF, Acros Organics, 99%). A 20 wt% SPEEK solution in DMF was prepared by using SPEEK polymer fibers with an equivalent weight (EW) of 500 g mol^{-1} SO_3H (Fumion® E-500, Fumatech, Germany). A separate solution of 15 wt% PFSA in DMF was prepared from a 25 wt% short-side chain (SSC) PFSA dispersion in water with an EW of 700 g mol^{-1} SO_3H (Fumion® FSLA-725, Fumatech, Germany). Appropriate amounts of DMF, SPEEK and PFSA solutions in DMF were then respectively added to an individually prepared 15 wt% PVDF-co-HFP (Kynar powerflex®

LBG, Arkema, France) solution in DMF. The compositions of the final dope solutions are summarized in Table 1.

The electrospinning process was conducted employing a wire-electrospinning setup (Nanospider NS LAB, Elmarco, Czech Republic). To ensure controlled conditions, the relative humidity and temperature of the electrospinning chamber were regulated using a desiccant dehumidifier system (DDS) (ML270PLUS, Munters, The Netherlands). The electrospinning process took place under $25 \pm 1\%$ relative humidity and 22 ± 0.5 °C. A distance of 25 mm was maintained between the collecting electrode and the substrate, while the substrate collecting speed was set at a constant rate of 5 mm min^{-1}. The blend solutions were subsequently subjected to wire-electrospinning, with a carrier (orifice diameter of 0.8 mm) moving along the working wire-electrode at a speed of 100 mm s^{-1}. An applied voltage of 80 kV was maintained between the working and collecting electrodes (with a working distance set at 170 mm).

Membrane fabrication

As presented in Fig. 1a and b, the single-layered membranes were fabricated by stacking 10 layers of electrospun fiber mats, all sharing the same SPEEK/PFSA/PVDF composition. These electrospun mats were meticulously aligned and stacked to reach a total thickness of 150 μm. Subsequently, the stacked layers were subjected to compression at 200 bar and 180 °C for 240 seconds. This process yielded transparent, compact membranes with a thickness spanning 30 μm to 60 μm. To prevent any distortion of the hot-pressed mats, a cooling down period was implemented involving the circulation of cooling water at 200 bar for 360 seconds.

The multi-layered membranes were prepared by initially stacking a single SPEEK-free electrospun mat, followed by three SPEEK-rich electrospun mats, all sharing identical compositions, and seven more SPEEK-free fiber mats, as illustrated in Fig. 1c. The 10 stacked layers then underwent the same hot-pressing process described above, yielding transparent and dense multi-layered membranes.

Subsequently, the membranes underwent a treatment process, which included immersion in a 1 M H_2SO_4 solution for 1 hour. This was followed by immersing the membranes in deionized (DI) water for an additional hour, adhering to the methodology described by Park *et al.*[19]

Fig. 1d shows the positioning of a single or multi-layered membrane within a single HBFB cell. For reference, the compositions of the electrospun mats used in the preparation of the hot-pressed membranes, along with the final SPEEK/PFSA/PVDF compositions, are listed in Table 2.

Table 1 Dope compositions for wire-electrospinning SPEEK/PFSA/PVDF blend fiber mats

SPEEK/PFSA/PVDF ratio (wt%/wt%/wt%)	Polymer concentrations (wt%)			
	Total	SPEEK	PFSA	PVDF
0/50/50	12	0	6	6
8/42/50	13	1	5.5	6.5
13/37/50	13	1.7	4.8	6.5
25/25/50	14	3.5	3.5	7
43/7/50	16	6.9	1.1	8

Table 2 Composition of the different blend fiber mats used for the preparation of dense membranes. SPFX-Y is used as the membrane code name, where SPF is the acronym for the SPEEK/PFSA/PVDF membrane, X shows the electrospun layer arrangement ($X = 1$ for single-layered and $X = 2$ for multi-layered membranes) and Y represents the total SPEEK content (wt%) in the final membrane

Membrane	Composition of the electrospun mats		Final SPEEK/PFSA/PVDF ratio (wt%/wt%/wt%)
	With SPEEK	Without SPEEK	
SPF1-0	—	0/50/50	0/50/50
SPF1-8	8/42/50	—	8/42/50
SPF2-8	25/25/50	0/50/50	8/42/50
SPF1-13	13/37/50	—	13/37/50
SPF2-13	43/7/50	0/50/50	13/37/50

Cross-section scanning electron microscopy (SEM) and energy-dispersive X-ray spectroscopy (EDS) analysis

All membrane samples were wetted in DI water, immersed in liquid nitrogen and then cryogenically fractured to visualize the cross-section with scanning electron microscopy (SEM). To avoid sample charging during imaging, the membrane samples were sputtered with platinum at 80 mA for 80 seconds under vacuum (JFC-2300HR, JEOL, Japan). Afterward, the cross-section morphology and elemental characterization of the prepared membranes were investigated using SEM (IT-100, JEOL, Japan) at 15 kV.

The elemental mapping of the membrane samples was performed with energy-dispersive X-ray spectroscopy (EDS) analysis. ImageJ software was employed to acquire the quantified intensity profiles.

For a better understanding of the data obtained from the cross-section EDS mapping of the single-layered (SPF1) membranes (Fig. 1a and b), the theoretically expected elemental composition of the SPF1 membranes with different SPEEK contents was also calculated and compared to the experimental results.

To obtain the average theoretical mass of fluorine (F, representative for PFSA and PVDF) in the SPF1 membranes, the following formula was used:

$$F^{Y}_{Theo.} = \frac{F^{0}_{Theo.} \times (50 - Y)}{50} \quad (3)$$

where $F^{Y}_{Theo.}$ (mg $g^{-1}_{Membrane}$) and $F^{0}_{Theo.}$ (mg $g^{-1}_{Membrane}$) are the average theoretical mass of F in the single-layered membranes containing Y (wt%) and 0 (wt%) SPEEK, respectively.

In addition, the average theoretical content of SO_3H groups, representing the sulfur (S) source of SPEEK in the blend membranes, was determined by the equation below:

$$S^{Y}_{Theo.} = M_W^{SO_3H} \times IEC^{Y}_{Theo.} \quad (4)$$

Where $S^{Y}_{Theo.}$ (mg $g^{-1}_{Membrane}$) is the average theoretical mass of S in the membrane containing Y (wt%) SPEEK. $M_W^{SO_3H}$ is the molar

mass of SO_3H (81.07 g mol^{-1}). $IEC^{Y}_{Theo.}$ (mmol SO_3H $g^{-1}_{Membrane}$) is the theoretical IEC value of the respective SPF1 membrane, which was calculated by eqn (5):

$$IEC^{Y}_{Theo.} = [Y \times IEC_{SPEEK} + (50 - Y) \times IEC_{PFSA}] \times 10^{-2} \quad (5)$$

where IEC_{SPEEK} is 2 mmol SO_3H g^{-1} SPEEK (EW_{SPEEK} = 500 g mol^{-1} SO_3H) and IEC_{PFSA} is 1.43 mmol SO_3H g^{-1} SSC PFSA ($EW_{SSC\ PFSA}$ = 700 g mol^{-1} SO_3H).

By employing the formulae above at a given SPEEK content (Y), the theoretical F/S mass ratio or $(F/S)^{Y}_{Theo.}$ was achieved by dividing $F^{Y}_{Theo.}$ by S^{Y}_{Theo}. The $(F/S)^{Y}_{Theo.}$ of each SPF1–Y membrane was separately compared to that of the SPF1-0 membrane using eqn (6):

$$(F/S)^{Y}\ \text{change}(\%) = \frac{(F/S)^{Y} - (F/S)^{0}}{(F/S)^{0}} \times 100 \quad (6)$$

Likewise, the experimental $(F/S)^{Y}$ change (%) was determined from eqn (6), in which the recorded data from the EDS mapping was used for $(F/S)^{Y}$ and $(F/S)^{0}$.

Membrane characterization

All membranse characterization measurements were repeated at least three times with fresh samples to ensure the reproducibility of the obtained data.

Ion exchange capacity

The number of functional groups in a membrane per unit weight of the dry membrane is indicated by the IEC. The standard method of acid exchange and base titration was used to determine the IEC of the membrane.[19] To do this, a membrane sample with an average dry weight of 20 mg was immersed in 100 mL of 1 M H_2SO_4 solution for 24 hours to protonate the membrane. Afterward, the sample was stirred in 100 mL of DI water for one hour to eliminate the surplus H_2SO_4 and then soaked three more times in separate 20 mL solutions of 1 M NaCl under stirring for 3 hours each. This was done to exchange H^+ for Na^+ ions. The amount of H^+ released into all three NaCl solutions was determined by titration with 0.01 M NaOH. The IEC of the membrane sample was then calculated:

$$IEC = \frac{N \times V}{m_{dry}} \quad (7)$$

where IEC (mmol SO_3H g^{-1} membrane) represents the ion exchange capacity of the membrane, N (mol L^{-1}) and V (mL) represent the normality and volume of the NaOH titrating solution, respectively and m_{dry} (g) demonstrates the sample's dry mass.

Swelling degree in 4 M HBr

The membrane swelling degree was assessed by immersing a membrane sample in a 100 mL bottle containing 4 M HBr solution for 24 hours. Afterward, the sample was stirred in 100 mL DI water for an hour, dried using a tissue and weighed using an analytical balance. The wet thickness of the membrane sample was also measured using a screw micrometer. The sample was then flushed with DI water three times to remove the excess HBr and oven-dried at 80 °C. The dry weight of the membrane was measured after this process. Using Formula (8), the membrane swelling degree in 4 M HBr (mg g^{-1} dry membrane) was calculated:

$$\text{Swelling degree in 4 M HBr} = \left[\frac{W_{wet} - W_{dry}}{W_{dry}}\right] \times 100 \quad (8)$$

The weight of the wet membrane sample is represented by W_{wet} (mg), while the weight of the dry membrane sample is represented by W_{dry} (mg).

Fixed charge density in 4 M HBr

The fixed charge density, which indicates the number of functional groups per volume of HBr solution in the membrane, explains the relationship between the IEC and the swelling degree. The fixed charge density (mmol SO_3H g^{-1} 4 M HBr) was determined using the following equation:

$$\text{Fixed charge density} = \frac{\text{IEC}}{\text{Swelling degree in 4 M HBr}} \times 1000 \quad (9)$$

Ionic conductivity

The membranes' ability to conduct ions (in this case, protons) in the through-plane direction was evaluated using alternating current (AC) impedance spectroscopy with a gold-stainless steel two-electrode cell having a 1 mm radius. The measurement was conducted using an SP-150 potentiostat from Bio-Logic, France. Before measurement, a membrane sample (10 mm radius) was soaked in a 100 mL solution of 4 M HBr for 24 hours and washed by stirring it in 100 mL DI water for one hour. The wet membrane was then clamped between two electrodes. The AC impedance measurement was performed at a frequency range of 10 000 Hz to 0.2 Hz and a constant voltage with a 10 mV sinus amplitude. Eqn (10) was used to compute the ionic conductivity (mS cm^{-1}):

$$\text{Ionic conductivity in 4 M HBr} = \left[\frac{t_{wet}}{(R_{total} - R_{blank}) \times A}\right] \times 10^{-1} \quad (10)$$

where the wet thickness is detonated by t_{wet} (μm). The resistance of the cell with and without the membrane is represented as R_{total} (Ω) and R_{blank} (Ω), respectively, and the active area of the electrodes is shown as A (cm^2).

Membrane electrochemical performance

The electrochemical performance of commercial PFSA and the prepared SPF membranes was tested in a single cell made of coated stainless steel with an active area of 64 cm^2 (Elestor, The Netherlands). The liquid diffusion electrode (LDE) in the cell contained one layer of 0.4 mm carbon cloth (Avcarb Material Solutions, US), while the gas diffusion electrode (GDE) contained a 0.2 mm carbon paper coated with 0.3 mg cm^{-2}

platinum–iridium (Pt–Ir/C, IRD Fuel Cells, Denmark) as the catalyst layer. The membrane was laminated to the GDE surface at 10 bar and 135 °C for 480 seconds. Two graphite bipolar plates (Eisenhuth, Germany) were separately positioned between the stainless-steel plate and the carbon electrode in each half-cell. To distribute the liquid electrolyte and hydrogen gas evenly through the porous carbon electrodes, an interdigitated and a serpentine flow field design (with constant channel depths of 1 mm) were grooved on one side of the bipolar plate facing the LDE and GDE, respectively. A 300 mL solution of 6.6 M HBr was used as the electrolyte and flowed through the cell at 50 °C with a flow rate of 110–130 mL min^{-1}. The hydrogen pressure during the charge and discharge phases was 0.5 bar and 0.3 bar, respectively. The temperature was maintained at a constant 50 °C throughout the experiment. To prevent gas pressure accumulation on the MEA and eliminate any crossover liquid on the gas side during charging, an automated purging system was regularly activated to remove the excess hydrogen from the negative half-cell.

Before initiating the electrochemical performance tests, the liquid electrolyte was circulated through the cell without any current flow for a duration of 2 to 6 hours to thoroughly soak the membrane with the HBr solution. The hydrogen pressure behind the membrane was kept above 0.3 bar to protect the catalyst by blocking HBr crossover from the liquid compartment.

Cell cycling measurement

Cyclic performance tests were carried out using an SP-150 potentiostat and a FlexP 0060 booster (Bio-Logic, France). The applied nominal current density was 0.2 A cm^{-2}. To avoid the accumulation of free Br_2 vapor, the maximum state of charge (SoC) was determined by reaching a minimum concentration of 1.5 M Br_2. The charging time required for the production of 1.5 M Br_2 was calculated using Faraday's law of electrolysis:[26]

$$C_{Br_2} \times V = \frac{I \times t}{n_e \times F} \quad (11)$$

where C_{Br_2} (mol L^{-1}) represents the Br_2 concentration that is either produced (at charging) or consumed (at discharge), V (L) is the electrolyte volume, I ((A) or (C s^{-1})) is the applied current, t (s) is the duration of the respective half-cycle, n_e refers to the number of moles of electrons (2) that is transferred by Br_2, and F (96 485 C mol^{-1}) represents the Faraday constant.

The voltage cut-off for the discharge phase was set at 0.6 V, while the voltage cut-off for the charge phase was the last recorded value at the end of the initial charge.

Open-circuit voltage and overpotential

The open-circuit voltage (OCV) refers to the potential difference observed between the positive and negative electrodes (LDL and GDL, respectively) when no current is flowing through the cell. To calculate the OCV from an HBFB charge–discharge curve, the points on the voltage curve where the current approaches zero correspond to the moments when the cell was neither charging nor discharging. By taking the average of these voltage points on the curve, the OCV was determined.

The overpotential (OP) during cycling represents the voltage deviation from its thermodynamic equilibrium value, indicating the energy losses or inefficiencies in the charge–discharge process. To calculate the charge overpotential ($OP_{Ch.}$) from the single charge–discharge curve, the obtained OCV was subtracted from the last voltage value recorded during the charging process. Similarly, the discharge overpotential ($OP_{Dis.}$) was considered as the difference between the last voltage value recorded during the discharging process and the OCV.

Bromine utilization

The bromine utilization in an HBFB cell refers to the degree of bromine species production and consumption during the charge and discharge processes, which can directly affect the energy capacity of the single cell. Bromine utilization within a single cycle can be determined by separately analysing the charge and discharge curves, applying Faraday's law as described in eqn (11).

Polarization

After charging the cell to 100% SOC (1.5 M Br_2) at a current density of 0.2 A cm^{-2}, the initial polarization measurement was conducted, followed by electrochemical impedance spectroscopy (EIS). This procedure was repeated three times, excluding the data recorded during the initial charging step from the subsequent evaluation. Cell polarization was assessed every 50 cycles. The current was stepped up or down until it reached a current density of ±600 mA cm^{-2}. This step was used to investigate the system's polarization behavior under varying current conditions. Every polarization test was repeated three times. The overall cell AR during charge and discharge was determined by calculating the average slope of the three current–voltage curves for each respective phase.

Electrochemical impedance spectroscopy

At the end of each cycle, electrochemical impedance spectroscopy (EIS) measurement was conducted at the OCV starting point using the signal sine mode. An alternating current with a sinus amplitude of 10 mV and a frequency ranging from 10 000 Hz to 0.2 Hz was used. Each measurement was 15 points each decade, with six measurements per point. The ohmic AR was calculated using the semi-circular Nyquist plot and the high-frequency intercept of the impedance with the real axis. The ohmic AR was calculated as the total of the cell compartment and electrode resistances, contact resistances, and membrane resistance. All EIS analyses were performed three times.

Cyclic efficiency and specific capacity

The coulombic and voltaic efficiencies as well as the energy capacity of the HBFB single-cell are derived from the analysis of the long-term cycling data using the following formulae:

$$\text{Coulombic efficiency}(\%) = \frac{I_{\text{discharge}} \times t}{I_{\text{charge}} \times t} \times 100\% \quad (12)$$

$$\text{Voltaic efficiency}(\%) = \frac{\int V_{\text{discharge}}\,\mathrm{d}t}{\int V_{\text{charge}}\,\mathrm{d}t} \times 100\% \quad (13)$$

$$\text{Specific capacity} = \frac{\text{Energy}}{\text{Volume}} \quad (14)$$

where specific capacity (Wh L^{-1}) quantifies the energy storage or output capability of the HBFB per unit volume of the electrolyte, Energy (Wh) is the amount of electrical energy stored or delivered during discharge and Volume (L) is the volume of the electrolyte in the battery.

Results and discussion

Cross-section morphology and elemental composition of dense membranes

The cross-section SEM images and EDS analysis of the hot-pressed SPF1 membranes are presented in Fig. 2a–c. The changes in the F/S ratio are plotted in Fig. 2d using eqn (6).

Fig. 2a–c show that by increasing the SPEEK content of the SPF1 membrane from 0 wt% to 8 wt% and further to 13 wt%, the cross-section texture of the membrane appears more wrinkled and uneven. This is due to the non-homogeneous blending between the hydrocarbon-based SPEEK and the fluorinated polymers, PFSA and PVDF.[23] A second phenomenon responsible for the imperfect surface could be the cryogenic fracturing of the samples before the SEM/EDS analysis.[20] It can be stated that the higher the SPEEK ratio, the rougher the surface, which in turn, can cause small variations in the X-ray collection by the detector from the sample. Nevertheless, the dense and hole-free appearance of all three membranes indicates that the incompatibility between SPEEK and PFSA/PVDF in the electrospun mats is counterbalanced by the applied high pressure and temperature during hot-pressing.[20]

It is also observed that by adding more SPEEK to the SPF1 composition, the average EDS-measured F/S intensity ratio decreases from ~2.14 to ~1.95 and ~1.20 for 0, 8 and 13 wt% SPEEK, respectively (Fig. 2a–c). Since SPEEK contains no F in its chemical structure, substituting the PFSA content with SPEEK results in a final mass reduction of $F_{\text{Theo.}}$ (eqn (3) and Table 3). As previously mentioned, SPEEK has a higher IEC than SSC PFSA. This implies that at a given final blend membrane weight, a gradual decrease of PFSA and an equal increase in SPEEK results in a higher $IEC_{\text{Theo.}}$ value (eqn (5) and Table 3). These changes, in turn, suggest a rise in the theoretical amount of SO_3H groups that are responsible for the transport of H^+ ions (eqn (4) and Table 3). Conclusively, by replacing PFSA with SPEEK in the SPF1 membrane at a given total mass while keeping the total PVDF amount at 50 wt%, the F and SO_3H contents decrease and increase, respectively. This causes a decline in the final theoretical F/S ratio (Theo. graph in Fig. 2d). A similar F/S reduction is obtained from the experimental data as more SPEEK is added to the SPF1 membrane (EDS graph in Fig. 2d). Slight variations in the slope of the EDS

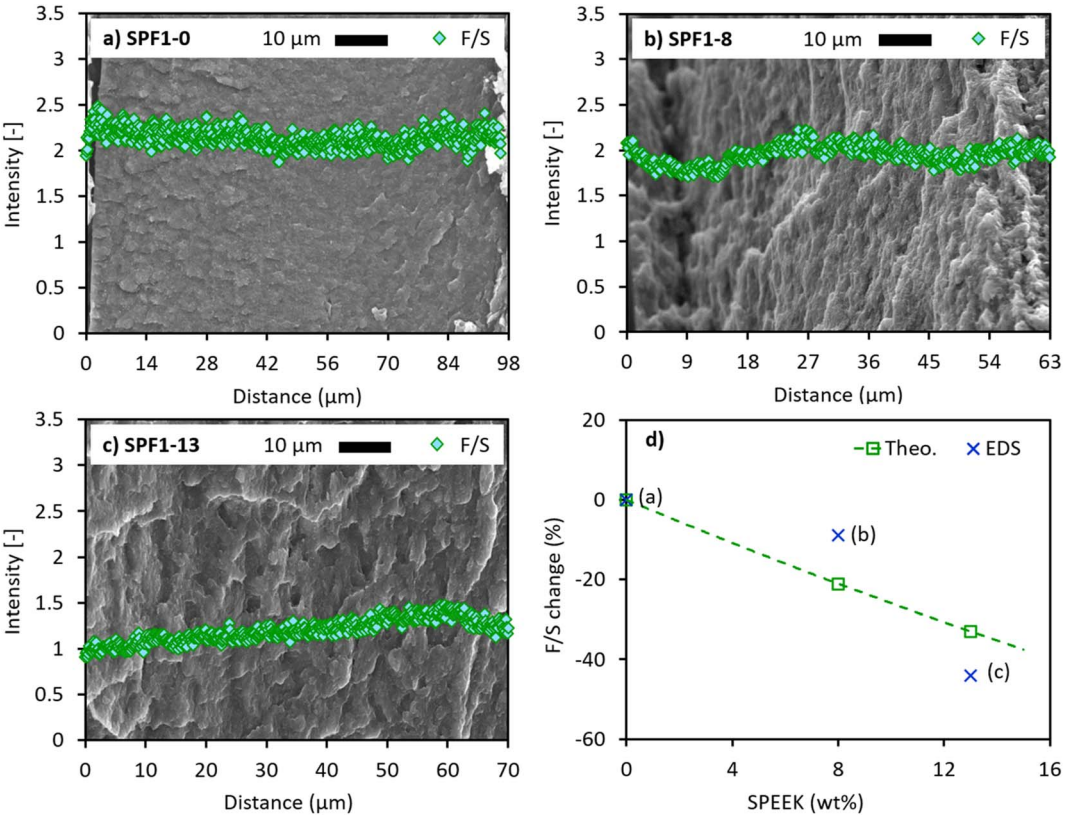

Fig. 2 Cross-section SEM images and EDS analysis of the hot-pressed SPF1 membranes: (a)–(c) F/S mass ratios obtained from the EDS analysis and (d) theoretical *vs.* EDS-measured change in the F/S ratios of the SPF1 membranes.

Table 3 The theoretical IEC of the SPF1 membranes as a function of the SPEEK content in the blend composition (eqn (5)), along with the changes in the theoretical F (eqn (3)) and S or SO_3H (eqn (4)) amounts per g of membrane

Membrane	$IEC_{Theo.}$ (mmol SO_3H g^{-1} membrane)	$F_{Theo.}$ (mg g^{-1} membrane)	$S_{Theo.}$ (mg g^{-1} membrane)
SPF1-0	0.71	1 $F^0_{Theo.}$	57.91
SPF1-8	0.76	0.84 $F^0_{Theo.}$	61.61
SPF1-13	0.79	0.74 $F^0_{Theo.}$	63.93

data from that of the theoretical data can be attributed to the non-ideal compression between the electrospun mats during the membrane preparation process.

Fig. 2a–c also show relatively constant F/S distributions through the thickness of the SPF1 membranes, confirming the identical polymer compositions of the stacked mats (Fig. 1a and b). The visibly small deviations in the F/S intensity profiles possibly stem from the slight composition difference between the electrospun mats.

Comparably, the cross-section SEM images and F/S intensity profiles of the SPF2 membranes are illustrated in Fig. 3.

Contrary to SPF1, the SPF2 membranes present heterogeneous F/S intensity distributions over the membrane thickness. The left and right-hand sides (thickness ~<4 μm and >~15 μm, respectively) of the SPF2 membranes show an almost two times higher average F/S intensity ratio than the middle area (thickness range of ~4–15 μm). This difference in the SPF2 elemental composition can also be observed in the cross-section morphology. In Fig. 3a, the left (distance <3 μm) and right (distance >13 μm) areas through the SPF2-8 thickness appear smoother and more uniform than the area between 3 μm and 13 μm distance. The relatively even surface and high average F/S ratio (1.72 ± 0.17) originate from the presence of PFSA-rich domain.[23,27] This implies that the mentioned regions are composed of hot-pressed 0/50/50 electrospun mats. This is why the middle zone (3–13 μm) exhibits a comparably rough structure and low average F/S value (0.91 ± 0.16), suggesting the ratio of 25/25/50 (Table 2) as the polymeric composition for the corresponding stacked layers. Similarly, the cross-section view and elemental profile of SPF2-13 (Fig. 3b) verify the intended layer arrangement (Fig. 1c) for the SPF2 membranes. However, it is shown that SPF2-13 retains less consistency in terms of cross-section morphology and F/S intensity distribution. Since the middle layers of the SPF2-13 cross-section (Fig. 3b) contain more SPEEK than those of the SPF2-8 membrane (43 wt% compared to 25 wt% in Table 2), the incomplete SPEEK blending with PFSA and PVDF during the electrospinning and hot-pressing becomes more significant. This results in a more pronounced diversity and instability in the through-plane membrane structure as well as the polymer distribution.

Membrane transport properties

The experimental characteristics of the investigated membranes are summarized in Table 4.

As seen in Table 4, all SPF membranes show a significantly lower IEC value than PFSA. This is due to the presence of PVDF in their structure which acts as an insulator against ion transfer.[5,20] By increasing the total SPEEK ratio in the SPF membranes from 0 to 8 wt%, the IEC increases by 10%, which further grows by 7% when the SPEEK concentration reaches 13 wt%. These results support the theoretically expected behavior for this parameter (Table 3). Moreover, the SPF2 membranes exhibit a slightly higher IEC compared to the SPF1 membranes at a given SPEEK content. The reason for this might be attributed to the middle layers of the SPF2 membrane containing a higher concentration of SPEEK, which due to its high swelling and IEC, facilitates the organization of hydrophilic regions in SPEEK and PFSA in a more accessible way for proton.[17] In contrast to SPF2, the absence of SPEEK-rich regions in the SPF1 membrane results in lower local values of IEC. In other words, not all of the SO_3H groups in the membrane may be readily accessible to the H^+ ions.

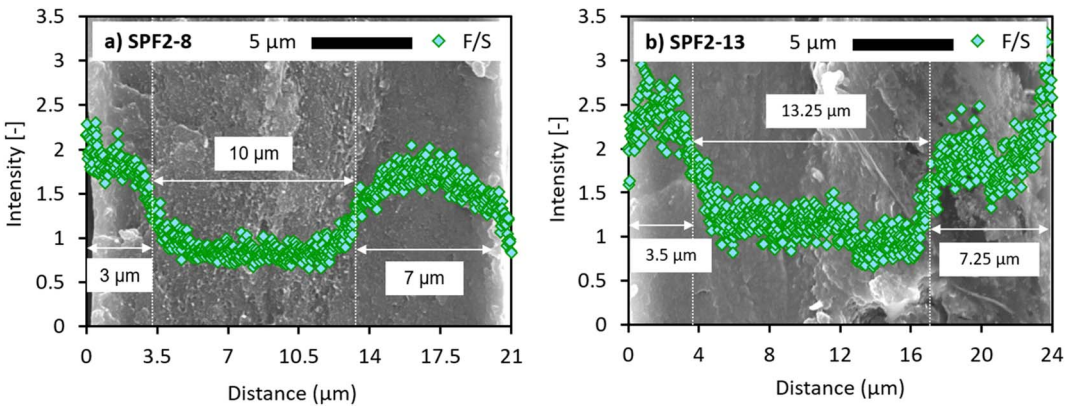

Fig. 3 Cross-section SEM images and F/S mass ratios obtained from the EDS analysis of (a) SPF2-8 and (b) SPF2-13 membranes.

Table 4 Characteristics of the PFSA and SPF membranes

Membrane	IEC (mmol SO_3H g^{-1} dry membrane)	Swelling degree in 4 M HBr (mg g^{-1} dry membrane)	t_{wet} (μm)
PFSA	1.20 ± 0.14	109 ± 6	125 ± 1
SPF1-0	0.54 ± 0.02	52 ± 3	94 ± 3
SPF1-8	0.57 ± 0.00	61 ± 6	62 ± 4
SPF2-8	0.61 ± 0.02	53 ± 2	42 ± 2
SPF1-13	0.62 ± 0.07	50 ± 4	28 ± 6
SPF2-13	0.63 ± 0.03	43 ± 6	41 ± 1

Table 4 also shows that the swelling degree of the SPF membranes in 4 M HBr is almost two times lower than that of the PFSA membrane. Similar to the IEC, this behavior is a result of the presence of 50 wt% PVDF in the SPF membrane structure, which limits the HBr uptake. On the other hand, the distinction between hydrophilic and hydrophobic regions in SPEEK is not as prominent as in PFSA.[17] Therefore, as the SPEEK content in the SPF membrane increases from 0 to 8 wt%, an 8% increase in the HBr uptake is observed. However, by further increasing the SPEEK content to 13 wt%, the swelling degree drops to a value lower than that of SPF1-0 (−11% decrease), implying insufficient compatibility between SPEEK and PFS.[28] This is further proved by the fact that at a given SPEEK ratio, the average swelling degree of SPF2 in 4 M HBr is ∼10% lower than its SPF1 counterpart, which is due to the high amount of SPEEK in their enclosed middle layers. The blending between SPEEK and PFSA becomes drastically lower as the compositional transition between hydrocarbon-free and hydrocarbon-rich domains in the SPF-2 arrangement (Fig. 1c) becomes sharper.[29]

Hence, for example, the SPF2-13 membrane can more effectively block any additional through-plane swelling than the SPF2-8 membrane.

The combination of higher IEC and lower HBr uptake of the SPF2 membranes compared to the SPF1 membranes at a given SPEEK ratio suggests that the multi-layer arrangement (Fig. 1c) is beneficial in creating a balance between these two parameters. Nevertheless, for a more conclusive comparison, the properties of the tested membranes in 4 M HBr, *i.e.*, the fixed charge density and the ionic conductivity, are visually represented in Fig. 4.

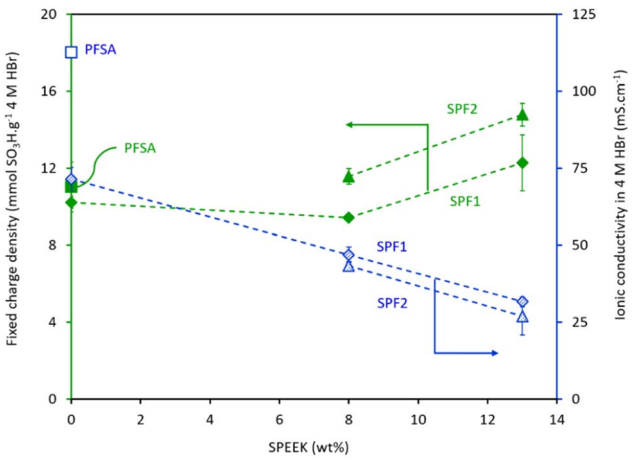

Fig. 4 Transport properties of the PFSA and SPF membranes: Fixed charge density and ionic conductivity in 4 M HBr. Lines are added to guide the eye but have no physical meaning.

Commercial PFSA displays a bit higher fixed charge density than the SPF1-0 and SPF1-8 membranes (Fig. 4). This suggests that the amount of available hydrophilic regions in the SPF1-0 and SPF1-8 membranes for proton transport is lower than in commercial PFSA.[5] As discussed earlier, the IEC increase of the SPF membranes is relatively smaller than the increase in their swelling degree as the SPEEK content increases from 0 to 8 wt%. This results in a slight decrease in the fixed charge density (Fig. 4). The observed increase in the fixed charge density by adding a total of 13 wt% SPEEK to the SPF membranes is an outcome of the considerably lower swelling degree in 4 M HBr of the membranes containing 13 wt% SPEEK than those with 8 wt% SPEEK (Table 4).

In general, a high fixed charge density is advantageous because it creates membrane channels for proton transport. Yet, it is intriguing to note that the ionic conductivity of the SPF membranes in 4 M HBr does not show an incline and even decreases going from 0 wt% to 13 wt% SPEEK, as seen in Fig. 4. As previously noted by Abbasi *et al.*[20] the proton conductivity of the pure SPEEK membrane is approximately 25% lower than that of pure PFSA in 4 M HBr. This variation in proton conductivity between SPEEK and PFSA membranes may be partially attributed to the clustering of hydrophilic SPEEK segments as discrete clusters, unlike the interconnected hydrophilic channels present in PFSA membranes.[17,30] In a homogeneous polymer composition, SPF membranes exhibit high consistency and evenness in the dispersion of their polymer chains, improving the membrane's fixed charge density.[5] However, while a high fixed charge density suggests more available hydrophilic areas within the membrane, it can be hypothesized that this is not necessarily translated into improved ionic conductivity. The higher the SPEEK content, the poorer the interfacial interaction between this hydrocarbon polymer and the partially fluorinated PFSA and PVDF. As suggested by Vezzù *et al.*,[31] the arrangement of water clusters within the electrospun PFSA/PVDF nanofibers is influenced by the size of hydrophobic domains. In other words, the water molecules in the hydrophilic domains of the membrane settle around the polar segments of the hydrophilic side chains of PFSA. This concept can be extended to the hydrophilic domains of SPEEK and PFSA interacting with the hydrophobic backbone of PFSA

and PVDF in the electrospun SPEEK/PFSA/PVDF membranes. Therefore, an increase in SPEEK content may enhance the interaction between the hydrophobic domains of PFSA and PVDF. As a result, this can potentially isolate the water clusters and reduce the ionic conductivity of the SPF membranes. Another tenable explanation is that since the sulfonic acid groups in the SPEEK-rich regions lack the selectivity and acidity of those in PFSA, the transport of protons becomes comparatively challenging in equal HBr concentrations.[32] This is also confirmed by the relatively lower ionic conductivity of the SPF2 membranes compared to the SPF1 membranes at a given SPEEK ratio.

Membrane performance in an HBFB cell

Area resistance. Fig. 5 presents the active area resistance (AR) of an HBFB cell over an extended period of operation, as measured by its polarization behavior and EIS while utilizing commercial PFSA and the prepared SPF membranes.

It should be emphasized that to establish a basis for long-term HBFB performance assessment, the electrochemical parameters used in this research were kept consistent across different membranes. The primary objective is to evaluate the performance and stability of the SPF membranes (with varied compositions, layer arrangements, and thickness ranges) over a prolonged period of time under identical electrochemical conditions rather than optimizing membrane characteristics and operational parameters for every membrane individually. Therefore, the SPEEK-containing membranes, according to their SPEEK content (Y), were prepared at a relatively lower thickness range than that of the commercial PFSA membrane. Consequently, a lower thickness decreases the resistance of the respective SPF membrane and enables the cell to cycle at a relatively higher current density (0.2 A cm^{-2} in this work). This approach also offers the advantage of reducing raw material costs through the utilization of thinner membranes (stacking fewer electrospun layers).

Additionally, it is noteworthy to mention that the electrochemical findings obtained from the SPF2-13 membrane sample (t_{wet} ~41 μm) were not included in this paper due to inadequate cell performance.

The commercial PFSA membrane (Fig. 5a) shows better performance (*i.e.*, lower AR) over 50 cycles than all the other membranes measured, due to the lack of non-conductive PVDF in the PFSA membrane.[6,19,20]

As mentioned earlier, more SPEEK leads to a higher through-plane resistance in the membrane, causing lower power output from the HBFB cell. Except for the SPF2-8 membrane (Fig. 5d), the resistance of all the tested membranes decreases by approximately 14% over time (comparing Cycle 1 and Cycle 50). Exposure to the HBr/Br_2 electrolyte gradually increases the diffusion coefficients of the membranes, facilitating the permeation of other ions than protons through the hydrophilic channels.[33] This reduces the AR (increases the membrane conductivity) during both polarization and EIS measurement.[32,34] In contrast, the SPF2-8 membrane shows an increase in total cell resistance due to a high local accumulation of SPEEK in the middle layers of the membrane (Fig. 1d). While SPEEK is inherently proton-conductive, its proton conductivity is notably lower than that of PFSA. Moreover, SPEEK is less stable in the HBr/Br_2 electrolyte compared to PFSA. Therefore, unlike the single-layered membranes, this SPEEK-rich middle section in the SPF2-8 membrane acts as a barrier to proton transport, minimizing the effect of longer contact with HBr/Br_2 electrolyte.[20,28,35]

Although the increased diffusion rate of the membranes in the acidic HBr/Br_2 medium improves the ionic conductivity, it can simultaneously lead to a higher uptake of bromine species. This is especially damaging to the SPEEK-rich membranes, as visible in *e.g.*, membrane SPF2-8, Fig. 5d, which are prone to bromine-induced degradation and consequently limit the cell lifetime.[20,35]

Additionally, the SPF1-13 membrane shows a relatively stable total resistance over 50 cycles (Fig. 5e), even though it contains a total of 5 wt% higher SPEEK content than the SPF2-8 membrane. This further indicates that sudden fluctuations in the SPEEK concentration profile through the blend membranes are detrimental to the membrane stability against the bromine species.

In other words, while preparing the SPF membranes, the single-layered electrospun mat arrangement (Fig. 1b) is preferred to the multi-layered stacking of the blend sheets (Fig. 1c) to ensure the durability/selectivity of the blend membrane at a given total SPEEK concentration.

All membranes show a decrease in their ohmic resistance (improved ionic conductivity) over time, except for the SPF2-8 membrane (Fig. 5d), which shows a 16% increase in the ohmic AR after 50 cycles. The degree of reductions in ohmic resistance of the single HBFB cell over 50 cycles (Fig. 5a–c and e) are 14%, 8%, 4% and 0% with the SPF1-8, PFSA, SPF1-0 and SPF1-13 membranes, respectively. The behavior of the ohmic resistance over 50 cycles is consistent with that of the total AR. This suggests that the total AR of the cell is largely influenced by the ohmic AR, which is primarily determined by the ionic conductivity of the membrane.

In general, the charge and discharge AR comparison exhibits a similar trend as the total and ohmic AR comparison, but with a comparatively lower rate of change (Fig. 5). Except for SPF2-8, all the membranes show a decrease in the amount of their charge and discharge AR values over 50 cycles. The average reduction rates of the AR, obtained from the polarization data during charge and discharge over 50 cycles, are 25%, 21%, 9%, and 8% for the SPF1-8, PFSA, SPF1-0 and SPF1-13 membranes, respectively. Oppositely, the average resistance of the SPF2-8 membrane obtained from the polarization measurement increases by 16% over 50 cycles, which is similar to that measured by the EIS analysis. A small improvement in the ohmic AR of the SPF1 and PFSA membranes can essentially be considered the main cause for the more noticeable enhancement in the polarization behavior of the HBFB cell over 50 cycles. Notably, the primary change in the SPF2-8 membrane is the substantial increase in the ohmic AR after 50 cycles, while the charge and discharge AR changes are comparatively smaller.

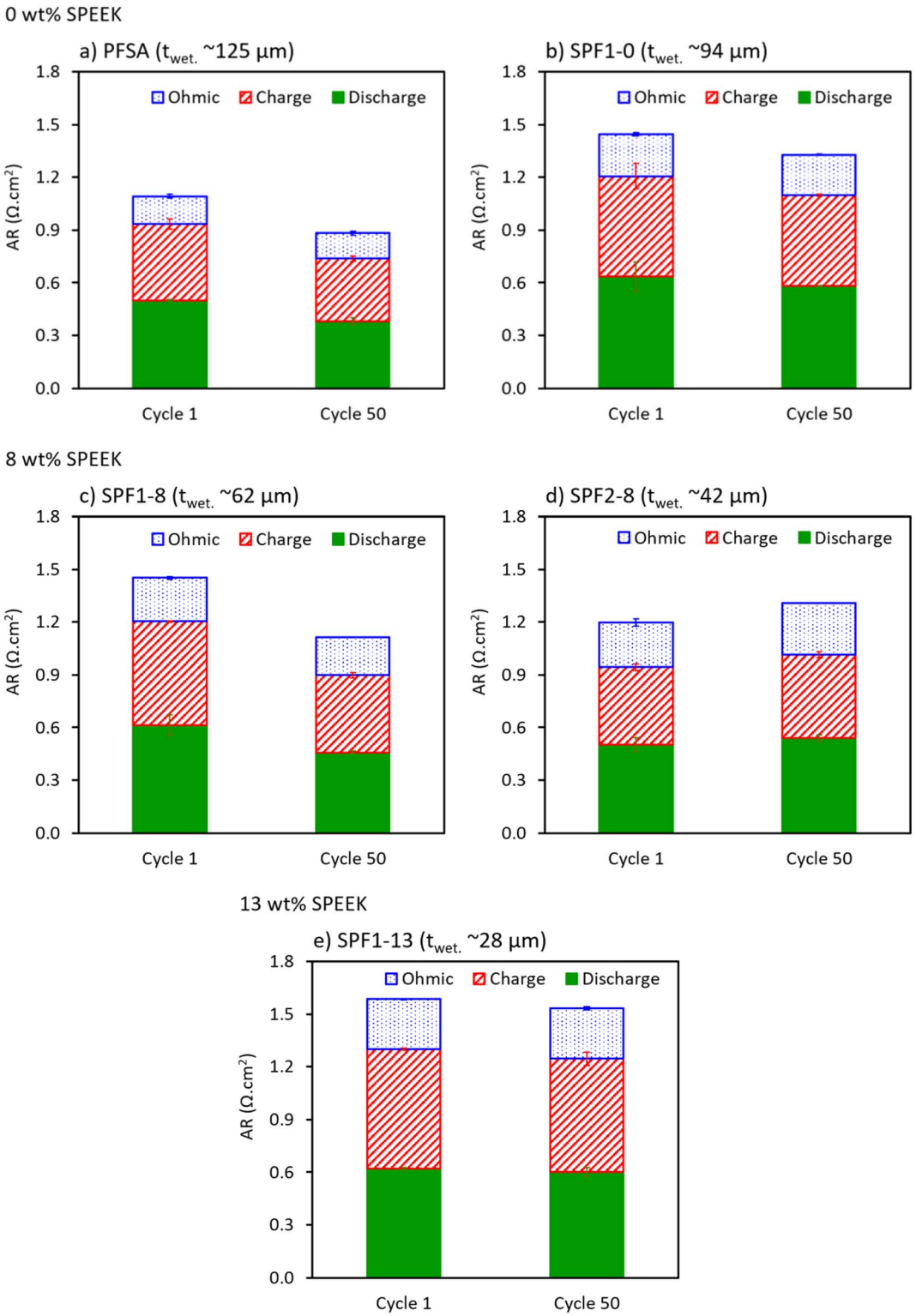

Fig. 5 The polarization and *in situ* EIS results of the HBFB single cell with the PFSA and the SPF membranes obtained after the cell's first full charge–discharge (cycle 1) and compared to those acquired after cycle 50. AR values after each specific cycle are evaluated based on the SPEEK content of their respective membranes: (a) 0 wt%; (b) 8 wt%; (c) 13 wt%.

Conclusively, the SPF1-8 membrane with a wet thickness of 62 µm (Fig. 5c) shows the best HBFB performance and durability over 50 cycles among the other tested SPF samples when compared to PFSA. The low thickness of the SPF1-8 membrane is also beneficial since it leads to significantly lower membrane costs than the commercial PFSA with a wet thickness of ≥120 µm.

It can be proposed that in order to achieve an equivalent HBFB polarization behavior to PFSA and maintain the cell

ohmic resistance sufficiently low, three key factors should be considered while preparing the SPF membrane with 50 wt% PVDF: (1) the thickness of the membrane should be reduced accordingly as more SPEEK is incorporated into it (referring to Table 4 and Fig. 5 as guidelines for the relationship between the SPEEK content and thickness/resistance of the SPF membranes); (2) the total SPEEK weight ratio should not surpass 13 wt%, with the recommended average being 10.5 wt% (averaging the SPEEK contributions within the SPF1-8 and SPF1-13 membranes, which respectively show the best and worst long-term resistance behaviors among the tested SPF membranes); and finally (3) the dense membrane should either have a uniform through-plane SPEEK distribution or a gradient through-plane polymer composition for a smooth transition between SPEEK-free and SPEEK-rich electrospun layers.[29]

Single-cycle performance comparison

Charge–discharge curves. Fig. 6 demonstrates the single charge–discharge performance curves of the tested membranes in the HBFB cell, measured at a current density of 0.2 A cm^{-2}.

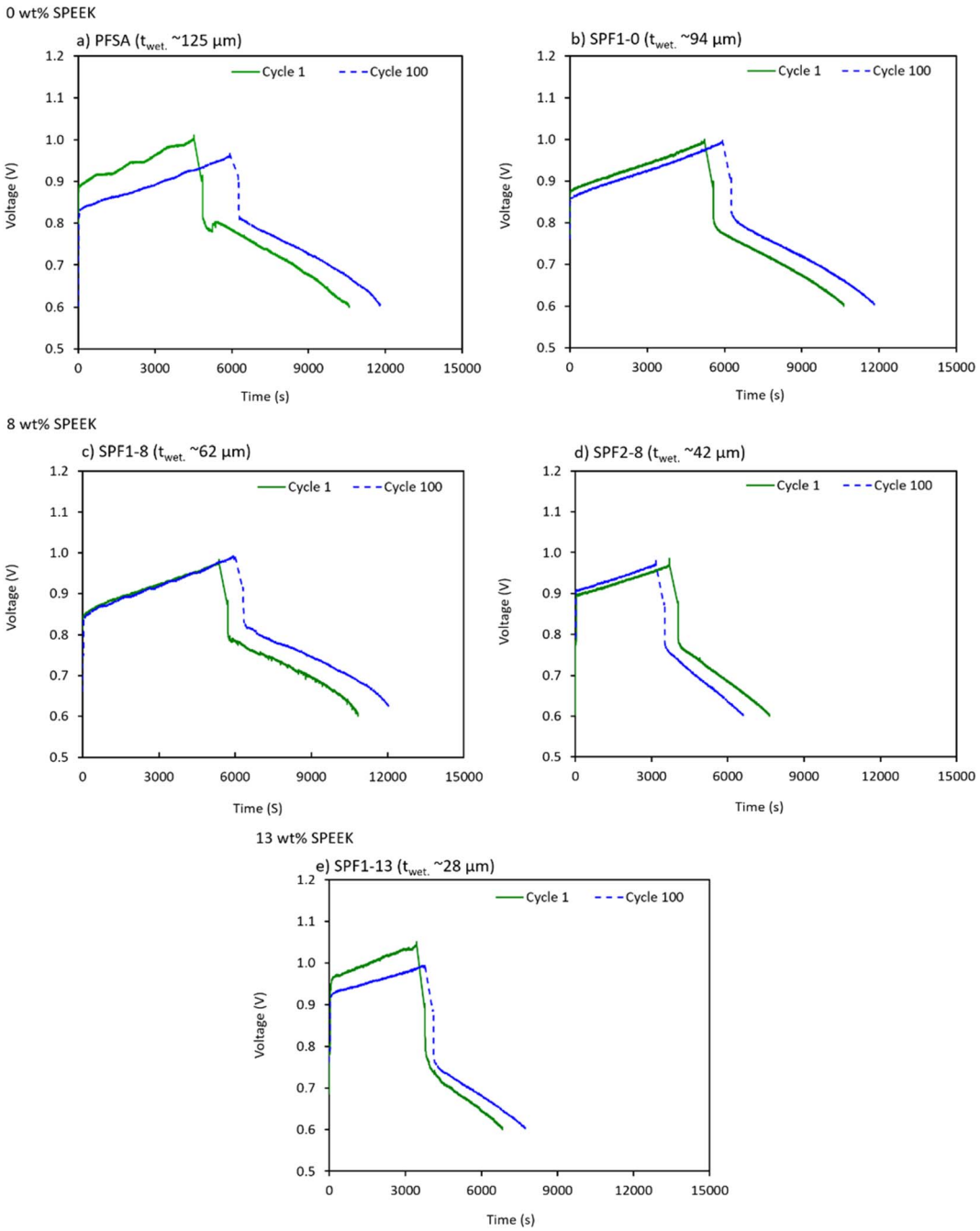

Fig. 6 Single charge–discharge curves of the HBFB cell with PFSA and the SPF membranes obtained from cycle 1 and cycle 100, separately: (a) and (b) 0 wt%; (c) and (d) 8 wt% and (e) 13 wt% SPEEK.

Based on the SPEEK concentration, the tested membranes are compared in terms of their cycling behavior. The 1st full cycle was compared to the 100th cycle for each cell for the purpose of long-term membrane performance evaluation.

The OCV, charge and discharge overpotential ($OP_{Ch.}$, $OP_{Dis.}$) corresponding to each membrane are extracted from cycle 1 and cycle 100 plots of the HBFB cell as shown in Fig. 6. The obtained values are presented in Table 5.

The OCV in an HBFB cell is primarily influenced by factors such as the operating conditions, hydrogen pressure, electrolyte composition and notably, the long-term crossover of bromine species through the membrane.[6] A higher level of bromine species crossover naturally translates into a lower permselectivity of the membrane and potentially a lower OCV. As anticipated, the HBFB cells utilizing membranes containing 0 wt% SPEEK (Fig. 6a and b) exhibit a nearly constant and highest OCV value of approximately 0.91 during 100 cycles (Table 5). This indicates a favorable balance between conductivity and permselectivity. In particular, the SPF1-8 membrane (Fig. 6c) shows an OCV of 0.88 V during the 1st cycle, but it is increased to 0.91 V during the 100th cycle (Table 5). This suggests an improvement in the membrane's transport properties over time as it becomes more saturated with the electrolyte, gradually leading to enhanced performance. The SPF2-8 membrane (Fig. 6d) exhibits the lowest OCV after 100 cycles compared to the other membranes, as seen in Table 5. This aligns with the earlier assumption regarding the degradation of locally accumulated SPEEK by the bromine species.[20] Furthermore, the OCV of the SPF1-13 membrane (Fig. 6e and Table 5) is slightly higher than that of the SPF2-8 membrane, supporting the significance of achieving a homogeneous through-plane SPEEK distribution to decrease the membrane crossover.

The charge–discharge OP is a measure of the additional energy required to drive the desired electrochemical reactions in the cell and can be primarily influenced by the ion transport properties of the membrane.[10] The ionic conductivity and permeability of the membrane directly impact the voltage losses, leading to OP during the cycling measurements. As seen in Fig. 6 and Table 5, the OP during charging ($OP_{Ch.}$) is larger than that during discharging ($OP_{Dis.}$) for all the tested membranes. This can be caused by the produced Br_2 and the associated mass transport limitations within the cell during charging.[8] As more bromine species cross over from the positive electrode through the membrane at charging, the available space on the catalyst electrode surface is reduced. Therefore, more activation energy is required to carry out the redox reactions, leading to a higher overpotential. It is also observed that over 100 cycles, the $OP_{Ch.}$ of all the cells is more affected over time compared to the OP_{Dis}. According to the presented results in Fig. 6 and Table 5, the commercial PFSA membrane demonstrates the lowest $OP_{Ch.}$ after 100 cycles.

The SPF1-13 membrane exhibits the highest $OP_{Ch.}$ values during both cycle 1 and cycle 100, indicating an inefficient ionic conductivity and limited mass transport at charging. Although the SPF2-8 membrane shows lower $OP_{Ch.}$ compared to the SPF1-13 membrane, the overall cycling performance of this membrane is reduced over 100 cycles. This can be caused by the imbalance between the conductivity and permselectivity of the SPF2-8 membrane due to its high local SPEEK concentrations in distinct domains. This also supports the results of the long-term polarization and EIS measurements in Fig. 5.

Ultimately, the HBFB cells employing the commercial PFSA, SPF1-0 and SPF1-8 membranes (Fig. 6a–c) exhibit the optimal charge and discharge OP values, along with the highest OCV over 100 cycles (Table 5). Consequently, longer cycle durations are also achieved with these membranes compared to the other tested cells (Fig. 6). Importantly, this also aligns with the polarization performance results (Fig. 5), providing further evidence that the SPF1-8 membrane (62 μm thick) can be considered a low-cost option with comparable performance to the relatively thicker PFSA and SPF1-0 membranes.

Bromine production and consumption

In addition to examining the voltage *vs.* time profiles, an additional approach to compare the cell performance of various membranes is by evaluating the bromine utilization throughout a complete cycle. The concentration of produced Br_2 at the end of charging (Produc. Br_2) and the amount of reacted Br_2 at the end of discharging (React. Br_2) with an active area of 64 cm^2 and a current density of 0.2 A cm^{-2} are obtained for the 1st and 100th cycles using eqn (11). The results are illustrated per membrane, in Table 6.

As seen in Table 6, throughout 100 cycles, all membranes demonstrate a marginally higher or predominantly constant Br_2 utilization, except for the SPF2-8 membrane, which aligns with the findings from Fig. 5 and 6. Aside from the SPF2-8

Table 5 The OCV and charge–discharge OPs obtained from the cycle 1 and cycle 100 curves in Fig. 6, corresponding to each membrane

	OCV (V)		$OP_{Ch.}$ (V)		$OP_{Dis.}$ (V)	
Membrane	Cycle 1	Cycle 100	Cycle 1	Cycle 100	Cycle 1	Cycle 100
PFSA	0.91	0.90	0.09	0.06	0.07	0.06
SPF1-0	0.90	0.91	0.10	0.09	0.07	0.07
SPF1-8	0.88	0.91	0.09	0.08	0.07	0.07
SPF2-8	0.87	0.88	0.10	0.09	0.09	0.08
SPF1-13	0.90	0.89	0.14	0.11	0.08	0.09

Table 6 Bromine utilization of the HBFB cell during charging (produc. Br_2) and discharging (react. Br_2) at 0.2 A cm^{-2} for cycle 1 and cycle 100 per tested membrane

	Produc. Br_2 (mol L^{-1})		React. Br_2 (mol L^{-1})	
Membrane	Cycle 1	Cycle 100	Cycle 1	Cycle 100
PFSA	1.00	1.31	1.26	1.22
SPF1-0	1.16	1.31	1.12	1.23
SPF1-8	1.19	1.32	1.13	1.29
SPF2-8	0.82	0.70	0.80	0.68
SPF1-13	0.76	0.83	0.68	0.80

membrane, the average production and consumption of Br_2 are increased by approximately 0.17 mol L^{-1} and 0.09 mol L^{-1}, respectively, over the span of 100 cycles. Furthermore, by excluding PFSA, the average production and consumption of Br_2 with the SPF1 membranes are increased by 0.12 and 0.13 mol L^{-1}, respectively. The improvement in the total bromine utilization suggests that the membranes progressively take up more electrolyte with longer cycling time, leading to a gradual increase in Br_2 usage.

For all the membranes, the amount of produced Br_2 per individual cycle is relatively higher than that of the reacted Br_2 (Table 6). This can be attributed to bromine species crossover through the membrane and a gradual loss of the amount of electrolyte. These factors may result in variations in the overall Br_2 concentration and the availability of ions for the electrochemical reactions during charge–discharge.[6,10]

According to Table 6, the cell with the SPF1-8 membrane exhibits the highest amounts of produced and reacted Br_2 (1.32 mol L^{-1} and 1.29 mol L^{-1}, respectively) during cycle 100. This is closely followed by an average of 1.31 mol L^{-1} production and 1.22–1.23 mol L^{-1} consumption of Br_2 with the PFSA and SPF1-0 membranes. Compared to the SPF1-0 and SPF1-8 membranes, the relatively lower amount of produced Br_2 with PFSA during cycle 1 may stem from insufficient membrane wetting due to the membrane's relatively high thickness. Conclusively, the HBFB cell bromine utilization that is achieved during the 1st and 100th charge–discharge cycles per membrane corroborates the voltage data obtained from the same cycle profiles in Fig. 6.

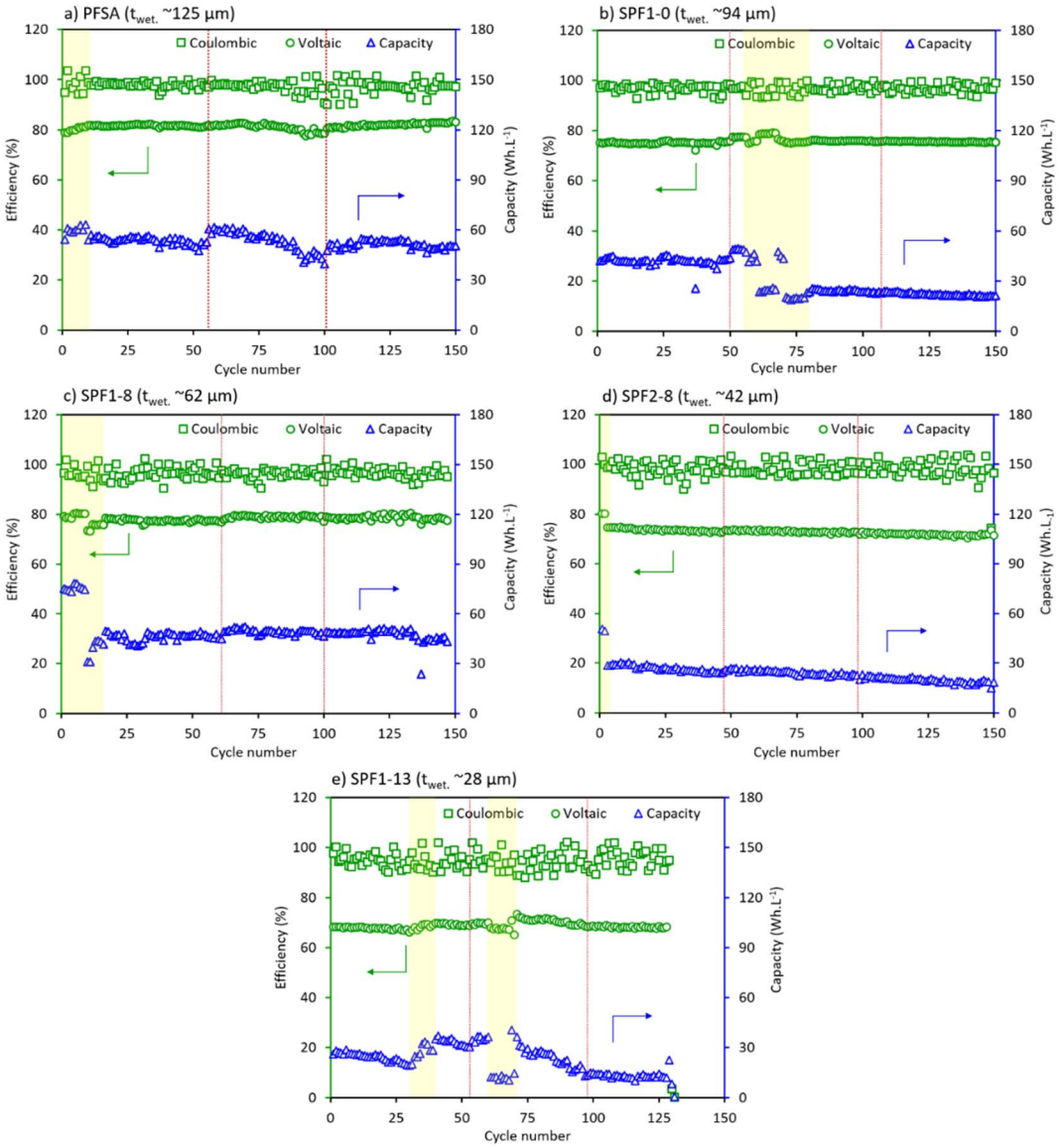

Fig. 7 The long-term cyclic efficiency and capacity of the HBFB single-cell with PFSA and the SPF membranes containing (a) and (b) 0 wt%; (c) and (d) 8 wt% and (e) 13 wt% SPEEK. The electrolyte refreshment instances are indicated by dotted vertical red lines, whereas the periods of externally/inherently induced fluctuations in the cell data collection are marked by yellow areas in the figure.

Long-term cyclic performance

The long-term cyclic performance of the HBFB single-cell with PFSA and the SPF membranes is compared in terms of the cell cyclic efficiency and capacity. The results over 150 cycles are illustrated in Fig. 7.

As shown in Fig. 7, the efficiency and capacity plots display scattered data points (areas marked in yellow). These data variations can be ascribed to experimental variability, environmental changes (*e.g.*, temperature and humidity) and the SPF membrane variability impacting chemical reactions and kinetics. Despite these variations, clear and distinct observations and associated conclusions can be obtained from these measurements. All membranes under investigation exhibit remarkably high coulombic efficiencies, nearly reaching 100% (Fig. 7). The coulombic efficiency displays a higher discrepancy when compared to the voltaic efficiency though, which is primarily due to the inevitable electrolyte crossover through the membrane. As more electrolyte diffuses from one cell compartment to the other during charging, the total Br_2 concentration reaches 1.5 M relatively sooner, leading to earlier termination of the charging process, as described in Table 5.[20] Although this disturbance in the HBFB cyclic performance is partially mitigated through the process of electrolyte renewal, the measured coulombic efficiency slightly surpasses 100% in most cases. This occurrence is suggestively due to an excessive amount of energy that is previously produced and becomes available for discharging later, leading to a slightly higher discharge capacity compared to the charge capacity.[5] More SPEEK content results in more electrolyte crossover through the SPF membrane. Hence, the efficiency trends become less stable and decrease over time (Fig. 7).

Fig. 7b indicates that SPF1-0 exhibits a relatively more consistent coulombic efficiency over 150 cycles than the PFSA membrane in Fig. 7a. However, the SPF1-0 membrane shows a relatively lower voltaic efficiency. This trade-off is attributed to the presence of PVDF, which increases the ohmic AR causing a decrease in voltaic efficiency. Simultaneously, PVDF obstructs the bromine species from crossing over to the hydrogen electrode, improving the coulombic efficiency.[5,6,20] The SPF1-8 membrane (Fig. 7c) demonstrates a more stable coulombic efficiency and a higher voltaic efficiency compared to the SPF2-8 membrane (Fig. 7d). This observation supports the previously suggested hypothesis concerning the accelerated degradation of locally-accumulated SPEEK in the SPF2-8 membrane (Fig. 5d and 6d). The non-uniform distribution of SPEEK through the SPF2-8 membrane is also responsible for the gradual decline in the cell voltaic efficiency over 150 cycles (high electrolyte crossover). Lastly, the SPF1-13 membrane (Fig. 7e) displays a comparatively scattered coulombic efficiency trend compared to the membranes containing 8 wt% SPEEK (Fig. 7c and d) (due to a higher total SPEEK content and a lower membrane thickness) and reduced voltaic efficiency (low ionic conductivity of SPEEK).[22]

Inevitable performance failure of the SPF1-13 membrane occurs around the 130th cycle, most likely attributed to catalyst corrosion induced by bromine species crossover through the membrane.

Similar to the cell efficiency graphs, increasing SPEEK results in a decline in both the average capacity and stability of the HBFB cell, as depicted in Fig. 7. The SPF1-0 membrane (Fig. 7b) shows significantly lower cyclic capacity than the PFSA membrane (Fig. 7a) due to the presence of insulating PVDF. Following the first electrolyte refreshment after 50 cycles (indicated by the dotted red line), the cell capacity with the SPF1-0 membrane decreases by 50%. After electrolyte refreshment, the cell cycling capacity temporarily drops due to factors such as initial equilibration of the new electrolyte, changes in chemical properties or concentrations and possible loss of active species.[15,36] The SPF1-8 membrane (Fig. 7c) demonstrates relatively high cyclic capacity in the first few cycles which is due to the initially elevated electrolyte flow rate that is subsequently adjusted to the original set value. After the manual adjustment of the electrolyte flow rate, the SPF1-8 membrane performance becomes mostly stable and higher than that of the SPF2-8 membrane (Fig. 7d). This demonstrates no acceleration in the degradation rate of the 8 wt% SPEEK content due to its even distribution through the membrane thickness (Fig. 1b). As previously explained, the SPF1-13 membrane (Fig. 7e) displays the poorest cyclic capacity and a complete failure after 130 cycles.

Conclusively, the SPF1-8 membrane with a thickness of 62 μm stands out as the best-tested SPF membrane with the best balance between the coulombic and voltaic efficiencies. Showcasing a stable and comparatively high capacity, the SPF1-8 membrane is the closest alternative to the benchmark PFSA membrane for use in HBFB.

Conclusions

We successfully developed dense membranes using wire-electrospun SPEEK/PFSA/PVDF blend fiber mats with the aim of contributing to a more economically friendly approach and exploring potential environmentally conscious alternatives for HBFB operation in the future. Firstly, we explored the impact of the SPEEK/PFSA/PVDF composition on the membrane properties and stability. Secondly, we investigated how the arrangement of electrospun layers with different polymer compositions affects the membrane performance and lifetime in an HBFB cell. The inherent incompatibility between SPEEK and PFSA/PVDF is effectively counterbalanced by wire-electrospinning and hot-pressing, resulting in dense and pinhole-free membranes. Nevertheless, higher SPEEK content leads to a less homogeneous through-plane membrane structure and a more heterogeneous polymer distribution. The insulating nature of PVDF in the SPF membranes gives a lower IEC and HBr uptake compared to PFSA. The multi-layer arrangement (attributed to the SPF2 membranes, which consist of distinctive SPEEK-rich and SPEEK-free regions) contributes positively to the blend membrane properties by achieving a better equilibrium between IEC (higher) and HBr uptake (lower) than the single-layer arrangement (present in the SPF1 membranes). While SPF membranes show consistent polymer chain dispersion and improved fixed charge density, their SPEEK-rich areas lack the selectivity and acidity of PFSA, leading to

reduced ionic conductivity. This noticeably applies to the multilayer membranes, due to their concentrated domains of SPEEK in the middle layers of the stacked membrane, in contrast to the homogeneous single-layer membranes at a given SPEEK ratio. A recommended average total SPEEK weight ratio of 10.5 wt% ensures an HBFB performance comparable to that of PFSA. Furthermore, the SPF membranes with uniform through-plane SPEEK distribution enable seamless ion uptake transition between SPEEK-free and SPEEK-rich domains. Long-term polarization behavior, cycling profile, and bromine utilization data over 100 cycles underscore the viability of the SPF1-8 membrane as the top-performing wire-electrospun SPEEK/PFSA/PVDF membrane with substantial capacity and stable coulombic and voltaic efficiencies. The SPF1-8 membrane presents a promising cost-effective and more environmentally favorable alternative to commercial PFSA for HBFB application by featuring reduced PFSA utilization (42 wt% of the total membrane weight) and half the thickness of commercial PFSA (62 μm).

Author contributions

Sanaz Abbasi: conceptualization, methodology, investigation, data curation, validation, visualization, writing – original draft, writing – review & editing. Yohanes Antonius Hugo: investigation, data curation, writing – review & editing. Zandrie Borneman: conceptualization, supervision, project administration, resources, writing – review & editing. Wiebrand Kout: supervision, funding acquisition, project administration, resources, writing – review & editing. Kitty Nijmeijer: conceptualization, supervision, project administration, resources, writing – review & editing.

Conflicts of interest

The authors confirm they have no identifiable conflicting financial interests or personal affiliations that might have influenced the research presented in this paper.

Acknowledgements

This project has received funding from the European Union's Horizon 2020 research and innovation programme under the Marie Skłodowska-Curie Grant Agreement no. 765289.

References

1 M. & Company, *Global Energy Perspective 2022: Executive Summary: McKinsey's Global Energy Perspective Is a Collaboration between Energy Insights and Adjacent Practices*, McKinsey & Company New York, NY, USA, 2022.
2 K. Amini, A. N. Shocron, M. E. Suss and M. J. Aziz, *ACS Energy Lett.*, 2023, 3526–3535.
3 K. T. Cho, P. Ridgway, A. Z. Weber, S. Haussener, V. Battaglia and V. Srinivasan, *J. Electrochem. Soc.*, 2012, **159**, A1806–A1815.
4 C. Roth, J. Noack and M. Skyllas-Kazacos, in *Flow Batteries*, Wiley, 1st edn, 2023.
5 Y. A. Hugo, W. Kout, A. Forner-Cuenca, Z. Borneman and K. Nijmeijer, *J. Power Sources*, 2021, **497**, 229812.
6 Y. A. Hugo, W. Kout, F. Sikkema, Z. Borneman and K. Nijmeijer, *J. Membr. Sci.*, 2018, **566**, 406–414.
7 T. X. Wang, M. D. Kelley, J. N. Cooper, R. C. Beckwith and D. W. Margerum, *Inorg. Chem.*, 1994, **33**, 5872–5878.
8 K. T. Cho, P. Albertus, V. Battaglia, A. Kojic, V. Srinivasan and A. Z. Weber, *Energy Technol.*, 2013, **1**, 596–608.
9 J. Masud, T. Van Nguyen, N. Singh, E. McFarland, M. Ikenberry, K. Hohn, C.-J. Pan and B.-J. Hwang, *J. Electrochem. Soc.*, 2015, **162**, F455–F462.
10 M. C. Tucker, K. T. Cho, F. B. Spingler, A. Z. Weber and G. Lin, *J. Power Sources*, 2015, **284**, 212–221.
11 N. Singh and E. W. McFarland, *J. Power Sources*, 2015, **288**, 187–198.
12 J. Woo Park, R. Wycisk, G. Lin, P. Ying Chong, D. Powers, T. Van Nguyen, R. P. Dowd Jr. and P. N. Pintauro, *J. Membr. Sci.*, 2017, **541**, 85–92.
13 R. S. Baldwin, *Electrochemical Performance and Transport Properties of a Nafion Membrane in a Hydrogen-Bromine Cell Eco*, 1987.
14 K. Oh, A. Z. Weber and H. Ju, *Int. J. Hydrogen Energy*, 2017, **42**, 3753–3766.
15 Y. A. Hugo, N. Mazur, W. Kout, F. Sikkema, Z. Borneman and K. Nijmeijer, *J. Electrochem. Soc.*, 2019, **166**, A3004–A3010.
16 Y. A. Hugo, W. Kout, F. Sikkema, Z. Borneman and K. Nijmeijer, *J. Energy Storage*, 2020, **27**, 101068.
17 K. D. Kreuer, *J. Membr. Sci.*, 2001, **185**, 29–39.
18 G. Lin, P. Y. Chong, V. Yarlagadda, T. V. Nguyen, R. J. Wycisk, P. N. Pintauro, M. Bates, S. Mukerjee, M. C. Tucker and A. Z. Weber, *J. Electrochem. Soc.*, 2016, **163**, A5049–A5056.
19 J. W. Park, R. Wycisk and P. N. Pintauro, *J. Membr. Sci.*, 2015, **490**, 103–112.
20 S. Abbasi, A. Forner-Cuenca, W. Kout, K. Nijmeijer and Z. Borneman, *J. Membr. Sci.*, 2021, **628**, 119258.
21 I. T. Kim, J. Choi and S. C. Kim, *J. Membr. Sci.*, 2007, **300**, 28–35.
22 Z. Li, J. Xi, H. Zhou, L. Liu, Z. Wu, X. Qiu and L. Chen, *J. Power Sources*, 2013, **237**, 132–140.
23 X. Liu, X. Meng, J. Wu, J. Huo, L. Cui and Q. Zhou, *RSC Adv.*, 2015, **5**, 69621–69628.
24 C. Klose, M. Breitwieser, S. Vierrath, M. Klingele, H. Cho, A. Büchler, J. Kerres and S. Thiele, *J. Power Sources*, 2017, **361**, 237–242.
25 B. Christgen, K. Scott, J. Dolfing, I. M. Head and T. P. Curtis, *PLoS One*, 2015, **10**, e0136108.
26 B. Liu, M. Zheng, J. Sun and Z. Yu, *J. Energy Storage*, 2019, **23**, 278–291.
27 A. Bagheri, M. Javanbakht, H. Beydaghi, P. Salarizadeh, A. Shabanikia and H. Salar Amoli, *RSC Adv.*, 2016, **6**, 39500–39510.
28 Y. Jiang, J. Hao, M. Hou, S. Hong, W. Song, B. Yi and Z. Shao, *Sustainable Energy Fuels*, 2017, **1**, 1405–1413.

29 H. Y. Jeong, D.-S. Yang, J. H. Han, J. Y. Lee, S. So, D. H. Suh, S. K. Hong, Y. T. Hong and T.-H. Kim, *J. Power Sources*, 2018, **398**, 1–8.
30 H.-Y. Jung and J.-K. Park, *Electrochim. Acta*, 2007, **52**, 7464–7468.
31 K. Vezzù, G. Nawn, E. Negro, G. Crivellaro, J. W. Park, R. Wycisk, P. N. Pintauro and V. Di Noto, *J. Am. Chem. Soc.*, 2020, **142**, 801–814.
32 A. Münchinger and K.-D. Kreuer, *J. Membr. Sci.*, 2019, **592**, 117372.
33 F. G. Will, *J. Electrochem. Soc.*, 1979, **126**, 36–43.
34 T. Wang, S. J. Moon, D.-S. Hwang, H. Park, J. Lee, S. Kim, Y. M. Lee and S. Kim, *J. Membr. Sci.*, 2019, **583**, 16–22.
35 Z. Yuan, X. Li, J. Hu, W. Xu, J. Cao and H. Zhang, *Phys. Chem. Chem. Phys.*, 2014, **16**, 19841–19847.
36 M. Küttinger, R. Riasse, J. Wlodarczyk, P. Fischer and J. Tübke, *J. Power Sources*, 2022, **520**, 230804.